Marija Đošić[1], Ana Janković[2], Kyong Yop Rhee[3], Vesna Mišković-Stanković[2,3,]*

[1]Institute for Technology of Nuclear and Other Mineral Raw Materials, Belgrade, Serbia, [2]University of Belgrade, Faculty of Technology and Metallurgy, Belgrade, Serbia, [3]Kyung Hee University, Department of Mechanical Engineering, Yongin, Republic of Korea

Review paper
ISSN 0351-9465, E-ISSN 2466-2585
UDC:620.197.5/.6
doi: 10.5937/ZasMat1802293D

Zastita Materijala 59 (2)
293 - 306 (2018)

Graphene reinforced hydroxyapatite biocomposite coatings obtained by electrophoretic deposition on titanium

ABSTRACT

Fast ongoing research of graphene-based nanomaterials reveals that their exceptional properties could be utized for biomedical applications, especially in tissue engineering and drug delivery. Here, we summarized the results obtained on hydroxyapatite based biocomposite coatings produced by electrophoretic deposition on titanium substrate and reinforced by nanosized graphene, as potential candidates for hard tissue implants.

Keywords: *electrophoretic deposition, coatings, biocomposites, hydroxyapatite, graphene.*

1. INTRODUCTION

Synthetic hydroxyapatite (HAP, $Ca_{10}(PO_4)_6(OH)_2$) is a widely used ceramic material for biomedical applications, due to the chemical similarity with mineral part of the human bones. However, materials' expected bioactivity and biocompatibility strongly depend on the crystallinity, porosity, particle size and surface area of the particles [1–4]. Bone fractures and bone diseases are commonly encountered in medical practice and often result in orthopedic surgery. For primary load-bearing purposes titanium and its alloys are materials of choice for long-term implant application due to their minimal impact on the surrounding body tissue (inflammation, allergic reactions) and favorable corrosion resistance, biocompatibility and good mechanical properties (e.g. strength, stiffness, toughness) [5,6]. In order to enhance bone healing process, biocompatibility of hydroxyapatite and excellent mechanical properties of titanium are usually combined to produce versatile bone implants [7,8]. Surface modification of titanium substrate by inorganic mineral coatings could be achieved by applying different techniques such as plasma spraying [9], sol-gel [10], biomimetic process [11], pulsed laser deposition [12] and electrophoretic deposition [13].

Corresponding author. Vesna Mišković Stanković
E-mail: vesna@tmf.bg.ac.rs
Paper received: 26. 04. 2018.
Paper accepted: 19. 05. 2018.
Paper is available on the website: www.idk.org.rs/journal

Thickness, morphology and porosity of coatings deposited on medical implants could be precisely controlled by electrophoretic deposition method [14–16]. However, HAP is a very brittle material and therefore needs to be improved in the form of a composite coating, especially since natural bone also consists of the mineral phase (apatite) and a polymer component (collagen). Development of HAP/biopolymer coatings that would mimic human bone is a very difficult task [16–19]. Natural polymers, such as chitosan/chitin, alginate, hyaluronic acid, collagen and silk, are considered suitable for the development of composite coatings with HAP, improving adhesion and reducing brittleness of pure hydroxyapatite coatings [19–26]. Chitosan (CS), widely used natural polymer, is semicrystalline homopolymer made up of β(1→4) linked N-acetyl-D-glucosamine and D-glucosamine sub-units [27]. The development of bioactive composites based on HAP and chitosan is of great interest. Chitosan possesses ability to stimulate bone repair and regeneration [28].

With the aim of assembling reinforced HAP biocomposites for load-bearing orthopedic applications, graphene (Gr) could be employed as a nanofiller, due to recent findings of its biological performance [16,17,29,30]. Two-dimensional carbon nanomaterial, Gr, possess extraordinary electrical, thermal and mechanical properties, as well as high specific surface area [31,32]. Graphene inclusion as nanofiller into polymer or ceramic matrices, remarkably improves mechanical properties of the host materials [31,33,34].

Additionally, mechanical properties and conductivity of chitosan can be modified by the graphene incorporation, because Gr controls the swelling rate of the chitosan [20]. From a biological point of view, Gr and Gr-based composites have low toxicity toward human osteoblasts [35], excellent antibacterial properties [36], and potential ability to initialize apatite mineralization [37].

However, problems regarding possible infections of bone implants, through bacterial adhesion to the implant surface and biofilm formation can lead to the body rejection of implant [38]. Trying to inhibit bacterial adhesion, the antimicrobial agent has to be added to the material for implantation [39]. The antimicrobial activity of silver and silver ions is well known for a very long time. Also, silver cations show low toxicity towards human cells [40,41]. For that reason, based on antimicrobial properties of Ag, great interest has been addressed to the development of silver doped HAP coatings for prevention of bone implant infections [21].

This article presents a comprehensive review of physico-chemical and biomedical characteristics of nanostructured biomaterials based on HAP, with addition of chitosan, graphene and/or silver, assembled on titanium substrates using electrophoretic deposition (EPD) method and targeted for development of novel hard tissue implants.

2. GRAPHENE DOPED HYDROXYAPATITE COATINGS

Modified chemical precipitation method was employed for synthesis of nanosized HAP powder [15]. The pristine hydroxyapatite, as well as hydroxyapatite/graphene (HAP/Gr) composite coatings were electrodeposited on Ti from absolute ethanol suspensions containing 1 wt.% of nanosized HAP (for HAP coating) and 1 wt.% of nanosized HAP and 0.01 wt.% of graphene (for HAP/Gr coating) using constant voltage method [16]. HAP/Gr bioactive coating, with improved mechanical strength and favorable corrosion stability in SBF solution was obtained.

The surface morphology of HAP and HAP/Gr composite coatings after air drying is shown in Fig. 1. HAP/Gr composite coating (Fig. 1a) had fewer cracks and no peeling off the Ti surface in the macroscopic observation, compared to the pure HAP coating (Fig. 1b), confirming that Gr effectively acts as a nano-reinforcement filler by preventing the creation and propagation of cracks. Bonding strength between graphene and HAP grain could be significantly enhanced due to high specific surface area of Gr nanosheets (GNSs) through an increased contact area with the matrix. Additionally, rough and wrinkled surface texture of Gr enhances mechanical interlocking [31] between coating and substrate. Also, two ends of the Gr nanosheet are well bonded to the adjacent HAP grains. Thus formed grain bridging that GNSs were providing could inhibit crack propagation along the grain boundaries.

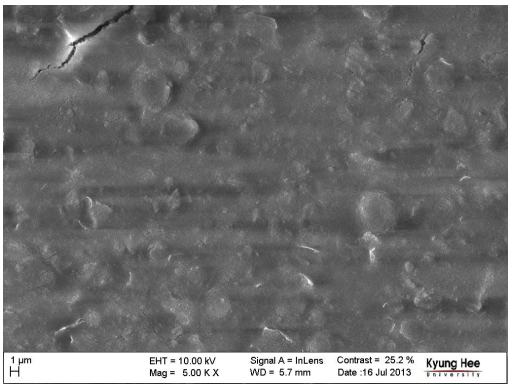

Figure 1. FE-SEM micrographs of the HAP/Gr (a) and HAP (b) coatings on titanium surface, magnification 5000x

Slika 1. FE-SEM mikrofotografije HAP/Gr (a) i HAP (b) prevlaka na površini titana, uvećanje 5000x

The FT-IR wavenumbers and corresponding assignments of absorption bands for HAP and HAP/Gr coatings are represented in Table 1. For HAP coating, characteristic bands at 1088, 1018 and 960 cm^{-1} in the ν_3 and ν_1 phosphate mode region could be observed due to the stretching of PO_4^{3-} ions [42]. The stretching band at 3570 cm^{-1} originates from free OH^- groups, while a broad peak at around 3375 cm^{-1} was noticed, due to H_2O adsorption. Clearly distinguished bands at 1089, 1024, and 962 cm^{-1} in the ν_3 and ν_1 phosphate mode region could be observed. Characteristic bands of HAP at 470, 560 and 601 cm^{-1} corresponding to P-O bending in phosphate group [43]. The presence of structural OH^- groups in the HAP lattice could be confirmed by characteristic band at 630 cm^{-1} [44]. The low intensity band at 875 cm^{-1} indicated the acidic phosphate group HPO_4^{2-} due to the P-(OH) stretching vibration

[45,46]. The bands in the range 1500–1400 cm^{-1} corresponded to ν_3 asymmetrical stretching vibrations of the CO_3^{2-} ions. The position of the carbonate bands indicated predominately substituted HAP of B-type. B-type HAP is present in human bones, having excellent bioactivity and osteoinductivity [47]. Graphene presence in the composite coating was confirmed by small bands at ~1540 cm^{-1} correspond to the skeletal vibration of Gr due to sp^2 hybridized C=C vibration stretching [43,48].

Table 1. FT-IR absorption bands of the HAP and HAP/Gr coatings on titanium surface

Tabela 1. FT-IR apsorpcione trake za HAP i HAP/Gr prevlake na površini titana

Coating	Group	Wavenumber / cm^{-1}	Assignment [42–48]
HAP/Gr	PO_4^{3-}	1089; 1024; 962	ν_3 and ν_1 phosphate mode region
		470; 560; 601	P-O bending in phosphate group
	OH^-	630	structural OH^- groups in the HAP lattice
	HPO_4^{2-}	875	P-(OH) stretching vibration
	CO_3^{2-}	1400–1500	ν_3 asymmetrical stretching vibrations of the CO_3^{2-} ions
	C=C	1540	skeletal vibration of graphene
HAP	PO_4^{3-}	1088, 1018, 960	ν_3 and ν_1 phosphate mode region
	H_2O	3375	H_2O adsorption
	OH^-	3570	vibration of the free OH^- group

The FT-IR analysis result stands in good agreement with the XPS results, confirming the presence of Gr in composite HAP/Gr coating. According to XPS analysis, the calculated Ca/P ratio of 1.58 for the HAP/Gr coating is greater than the Ca/P ratio for the pure HAP coating of 1.50 and closer to the stoichiometric value [16].

Based on the experimental results obtained from SEM, FT-IR and XPS analyses, the formation of the composite HAP/Gr coating was confirmed, even there is no obvious evidence indicating the chemical reaction between HAP and graphene sheets [16]. This is in good agreement with literature, where the interaction between HAP and graphene could be explained by Van der Waals bonding [49]. Nucleation of HAP crystals probably originates on either the graphene wall or the cross-section of graphene multi-sheets, followed by crystal propagation along or perpendicular to the surface of the graphene sheet. Crystal planes of HAP form a strong interfacial bond with the surface of Gr wall and the cross-section of Gr builds a stronger interface with HAP crystal planes due to the smaller lattice mismatch. As a consequence, the less cracked morphology was observed (Fig. 1) on the HAP/Gr coating surface compared to pure HAP coating. Graphene incorporation influences also the thermal stability of electrodeposited coatings [16]. From TGA curves the total weight loss for the HAP coating was calculated to be 7.16 wt.% and for HAP/Gr coating 5.28 wt.%, confirming the greater thermal stability of HAP/Gr coating.

The formation of a bone-like apatite layer on the surface of bioactive materials occurred after immersion of the HAP and HAP/Gr coatings in SBF solution, at 37 ºC for 7 days, confirming the high bioactivity of HAP and HAP/Gr coatings [16]. Using XRD method, this was confirmed by the shifting of the HAP characteristic diffraction maxima toward higher angles, meaning that after immersing of the HAP and HAP/Gr composite coating in SBF, carbonate ions incorporate into the apatite lattice by occupying the OH^- sites or the PO_4^{3-} position [31,50], forming the bone-like apatite. Additionally, even small amount of graphene addition causes the formation of HAP crystallite with smaller crystallite domain size, which is highly beneficial for bioactivity of coatings.

The mineralization process of newly formed HAP proceeds occur through dissolution of phosphate and calcium ions from the HAP and HAP/Gr coatings [31]. Dissolution process accelerates on the surface of the HAP/Gr coatings due to the presence of Gr on the grain boundaries, resulting in smaller grain size of coatings and improved interaction with SBF. In the second step precipitation of an apatite layer occurs. This can be explained as follows: in SBF, the surface of HAP/Gr coatings is negative due to dissolution of calcium ions, elevating in the same time the concentration of calcium ions in SBF. The conditions for formation of a Ca-rich layer are fullfield. Newly formed Ca-rich layer penetrating the whole HAP/Gr coating surface. The third stage is the final formation of apatite as the Ca-rich layer attracts phosphate ions from the SBF and forms bonelike apatite clusters.

To predict the bone implant behavior *in vivo*, corrosion stability of the biocomposite HAP/Gr coating, as well as HAP coating, was evaluated in SBF at 37 ºC by EIS measurements [16].

Impedance spectra for HAP/Gr and HAP coatings in the Nyquist plots during immersion in SBF were fitted by equivalent electrical circuits (EECs) represented in Fig. 2, where CPE_c is the constant phase element of the coating, CPE_{ox} is the constant phase element of the passive oxide layer on the Ti surface beneath the coating, R_s is the electrolyte resistance and R_c is the coating pore resistance. The values of EECs for HAP/Gr and HAP coatings are represented in Table 2.

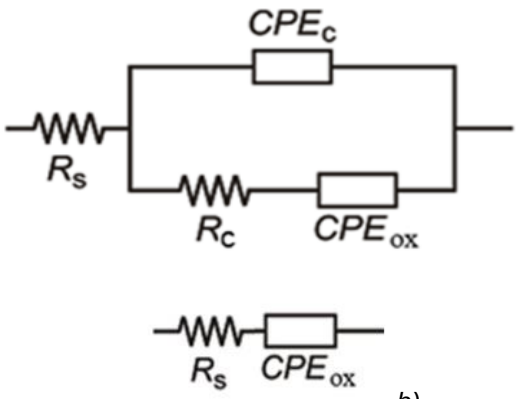

Figure 2. Equivalent electrical circuits used for impedance plots fitting of the HAP and HAP/Gr coatings on titanium surface during different immersion times in SBF at 37 ºC (a) and at the end of experiment (b)

Slika 2. Ekvivalentna električna kola korišćena za fitovanje impedansnih dijagrama za HAP i HAP/Gr prevlake na površini titana, tokom vremena delovanja SBF na 37 ºC (a) i na kraju eksperimenta (b)

For the HAP/Gr composite coating, during initial 48 hours, SBF solution diffused into the coating pores and filled them out, which can be detected by decreasing of R_c value from 12.5 to 3.7 kΩ cm^2 (Table 2). During the third day, the beginning of the biomineralization process occurred by the formation of a new apatite layer onto the HAP/Gr surface, which was detected by increasing in R_c to the value of 5.0 kΩ cm^2. Finally, after 13 days of immersion in SBF solution the coating pore resistance increased to 34.2 kΩ cm^2, i.e. bioactivity was observed. After 15 days of immersion, when coating adhesion loss had occurred, HAP/Gr coating surface represented a site of nucleation and growth for a new apatite layer recognized as carbonated HAP.

Compared to the HAP/Gr coating, pure HAP coating formed new apatite layer during the initial 8 hour period (Table 2), which was proved by increase in R_c from 12.7 kΩ cm^2 (after 1h immersion) to 15.0 kΩ cm^2 (after 8 h immersion). For longer time of immersion in SBF, after 24 h, HAP coating lost its corrosion stability.

Advantages of graphene incorporation in HAP structure of composite HAP/Gr coating could be clearly observed through the superior biomimetic mineralization, compared to pure HAP coating.

Table 2. Coating pore resistance, R_c, of the HAP and HAP/Gr coatings on titanium surface

Tabela 2. Otpornost u porama prevlake, R_c, za HAP i HAP/Gr prevlake na površini titana

Sample	*t*/h	R_c / kΩ cm^2
HAP/Gr	1	12.5
	7	7.6
	24	3.9
	48	3.7
	72	5.0
	312	34.2
	360	-
HAP	1	12.7
	6	15.6
	8	15.0
	24	-

Cell survival in the presence of HAP/Gr composite coatings on Ti was determined using a standardized MTT test [16]. Cell survival against healthy peripheral blood mononuclear cells (PBMC) was 72.3±4.3%. Examination of the cytotoxic effects showed a mild decrease in the survival of healthy immunocompetent PBMCs compared to the control cell sample. According to materials cytotoxicity classification, HAP/Gr composite coating could be considered non-cytotoxic within the margin of error against targeted PBMCs.

The antibacterial activity of HAP/Gr coating was tested against *S. aureus* TL and *E. coli* (ATCC 25922) in suspension using the spread-plate method in phosphate buffer (PB) [16]. The antibacterial activity of Gr itself is controversial and demands further investigation. No antimicrobial activity of the HAP/Gr composite coating could be noticed immediately after inoculation of samples. Cell viability remained at the same level as observed up to 3 h post incubation when compared to the initial number of cells in suspension. After 24 h of exposure noticeable bacterial growth was evident in case of both bacteria. Based on the presented data, HAP/Gr coatings exhibited no reduction of *S. aureus* TL or *E. coli* after 24 h. The same behavior of *S. aureus* TL was reported for a pure HAP coating [51].

3. SILVER DOPED HYDROXYAPATITE AND HYDROXYAPATITE/GRAPHENE COATINGS

Antibacterial coatings on titanium, containing inorganic antimicrobial agents, silver in particular, are known for their excellent biocompatibility and stability [17]. As doping agents, silver and silver ion inhibits bacterial attachment onto surface of biomaterials during initial period. Additionally, silver and/or silver ions have broad antibacterial spectrum and excellent biocompatibility without genotoxicity or cytotoxicity. Graphene was added to Ag/HAP coatings with the aim to explore potential influence of Gr implementation as reinforcement of antimicrobial coatings.

Electrophoretic deposition was performed from absolute ethanol suspensions containing 1wt% of nanosized Ag/HAP powder (Ag/HAP coatings) or 1wt% of nanosized Ag/HAP powder and 0.01wt% of Gr (Ag/HAP/Gr coatings), using constant voltage method [17].

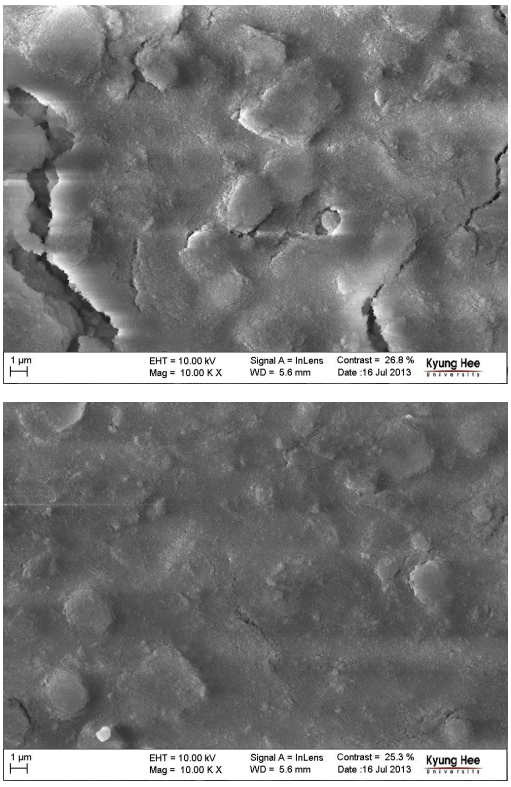

Figure 3. FE-SEM micrographs of the Ag/HAP (a) and Ag/HAP/Gr (b) coatings on titanium surface, magnification 10000x

Slika 3. FE-SEM mikrofotografije Ag/HAP (a) i Ag/HAP/Gr (b) prevlaka na površini titana, uvećanje 10000x

The SEM microphotograph of the surface morphology of the Ag/HAP and Ag/HAP/Gr coatings, electrodeposited on titanium, is shown in Fig. 3. On the Ag/HAP coating surface (Fig. 3a), micro-cracks appeared, most probably as a consequence of shrinking during air drying. Also, a lot of agglomerates on the coating surface would benefit the overall porosity. Osteointegration and osteoconduction properties can be enhanced using the porous apatite layers [52]. It has been reported that penetration of the surrounding bone tissue through the open interconnected pores is advantageous, enabling better biointegration of surrounding bone and coated implants [53]. Compared to the Ag/HAP coating (Fig. 3a), the Ag/HAP/Gr composite coating had fewer cracks (Fig. 3b). This can be explained by the interaction of HAP lattice and graphene sheets through the bonding mechanism, as was described for HAP/Gr coating (section 2). Graphene addition, as nano-reinforcement filler, prevents and suppresses cracks propagation. Also, graphene has a great impact on brittle materials through the toughening effect by frictional pull out, crack deflection, and crack bridging [31], retaining HAP original biocompatibility as well.

The FT-IR wavenumbers and corresponding assignments of absorption bands for Ag/HAP and Ag/HAP/Gr coatings are represented in Table 3. In both spectra, characteristic hydroxyapatite bands could be detected [37,54]. All bands at FT-IR spectrum of electrodeposited Ag/HAP coating on titanium correspond to the hydroxyapatite [15,17]. The broad bands at 3000–3500 cm^{-1}, stretching vibration band at 3572 cm^{-1} and the bending mode at 1613 cm^{-1}can are assigned to O–H stretching and bending of H_2O in the Ag/HAP coating [55]. The band in the region from 1216–920 cm^{-1} can be assigned to the P–O asymmetric stretching mode (ν_3) vibration of the PO_4^{3-} group [15,56]. In the region from 635 to 500 cm^{-1}, strong peaks observed as the doublet, was derived from the triple (ν_4) degenerated bending modes of phosphate O–P–O bonds [57]. One weak band at 636 cm^{-1} corresponds to the vibration of structural OH– groups in the hydroxyapatite lattice [44]. The presence of HPO_4^{2-} group in the crystal lattice was identified by the small sharp peak at 876 cm^{-1} [15]. Transformation of the single band in ν_4 region of PO_4^{3-} group to a doublet band indicates the improvement of the HAP crystallinity [42,57]. It can be concluded that incorporation of Ag into HAP structure improved crystallinity of Ag/HAP coatings, making it as a suitable surface for proliferation of bone cells.

For Ag/HAP/Gr composite coating [17] FT-IR bands at 1089, 1024, 962, 601, 560 and 470 cm^{-1} can be assigned to stretching and bending of phosphate groups in hydroxyapatite. Band at 875 cm^{-1} can be assigned to acidic phosphate group, HPO_4^{2-} ions in the Ag/HAP/Gr [46]. Weak band at

630 cm^{-1} corresponds to the vibration of structural OH– groups in the hydroxyapatite lattice. Bands in the region from 1500 to 1200cm^{-1} correspond to stretching vibrations of CO_3^{2-} ions in the HAP, indicating prevalance of B-type hydroxyapatite. This kind of carbonate substituted hydroxyapatite is advatageous in the human bone due to excellent bioactivity and osteoinductivity [47]. Absorption bands located at ~1540 cm^{-1} in the FT-IR spectrum of Ag/HAP/Gr composite coatings correspond to the skeletal vibration of Gr [17,58].

Table 3. FT-IR absorption bands of the Ag/HAP and Ag/HAP/Gr coatings on titanium surface.

Tabela 3. FT-IR apsorpcione trake za Ag/HAP i Ag/HAP/Gr prevlake na površini titana.

Coating	Group	Wavenumber / cm^{-1}	Assignment [15,17,37,44,46,54–58]
Ag/HAP	OH^-	3572	stretching vibration of OH^-
	H_2O	1613	bending mode of H_2O
	PO_4^{3-}	1216 - 920	P–O stretching in phosphate group
		635 - 500	bending of phosphate O–P–O bonds
		636	structural OH^- groups in the HAP lattice
	HPO_4^{2-}	876	acidic phosphate group
Ag/HAP/Gr	PO_4^{3-}	1089, 1024, 962, 601, 560, 470	stretching and bending of phosphate groups in HAP
	HPO_4^{2-}	875	acidic phosphate group
	OH^-	630 cm^{-1}	structural OH^- groups in the HAP lattice
	CO_3^{2-}	1200-1500	stretching vibrations of the CO_3^{2-} ions
	C=C	1540	skeletal vibration of graphene

Thermogravimetric analysis was employed to evaluate thermal stability of Ag/HAP and Ag/HAP/Gr composite coatings. Total weight loss for the Ag/HAP/Gr coating in the temperature range of 25-1000°C was 7.12 wt. % [17], confirming the greater thermal stability of Ag/HAP/Gr coating compared to Ag/HAP coating as a reference, where mass loss was 7.90 wt% [15]. The thermal stability of Ag/HAP/Gr coating was substantially improved as a consequence of bonding mechanism between graphene sheets and hydroxyapatite lattice.

XRD pattern of Ag/HAP coatings confirmed incorporation of silver ion in the hydroxyapatite crystal lattice [17], through the substitution of calcium ions. Incorporated Gr influences the particle size, e.g. smaller particle size of the Ag/HAP/Gr coating was found (17.6 nm) [17] in respect to Ag/HAP (35.2 nm) [59]. Also, the incorporation of silver ion in the hydroxyapatite crystal lattice, as well as interaction of graphene with HAP lattice can be confirmed from the XRD pattern for Ag/HAP/Gr coatings, where characteristic diffraction maximums for Ag and graphene can be observed [15,17]. The XPS results revealed the presence of Ag element in both Ag/HAP and Ag/HAP/Gr coatings [17]. Graphene incorporation in Ag/HAP/Gr coatings was confirmed by XPS analysis, detected with C1s peak that could be attributed to aromatic hydrocarbons [60], actually C=C sp^2 bonds in the graphitic network. Incorporation of graphene in Ag/HAP/Gr coating, provided an optimal Ca/P ratio of 1.52, enabling succesful bone integration with biomaterial [17], while the Ca/P ratio for silver doped hydroxyapatite Ag/HAP coating was calculated to be 1.50 [15].

The bioactivity of Ag/HAP/Gr coating, e.g. ability of formation of bone-like apatite, was tested by immersion in SBF solution at 37 ºC for 7 days. Formation of carbonated HAP layer on the Ag/HAP/Gr coating surface upon soaking in SBF was confirmed by XRD and FE-SEM [17] and indicated its high bioactivity. Upon immersion of the Ag/HAP/Gr coating in SBF, carbonate ions incorporate into the apatite lattice by occupying the OH^- sites or the PO_4^{3-} position, forming the bone-like apatite [17]. Highly porous surface structure of newly formed HAP enables better connection between the implant and the bone. It has been reported that open interconnected porosity structures facilitate penetration of the surrounding bone tissue and hence lead to better biointegration and mechanical stability.

The corrosion stability of Ag/HAP and Ag/HAP/Gr coatings was studied in SBF solution by EIS after 0, 11, and 24 days in SBF at 37 ºC [17]. The experimental impedance data of Ag/HAP/Gr coating and Ag/HAP coating are presented in Table 4. Fitting of experimental data was accomplished by using the equivalent electrical circuits (EECs) shown in Fig. 2. Obtained fitting values for each EEC parameter, as well as Nyquist plots for both Ag/HAP/Gr and Ag/HAP coatings are, represented and discussed in details in literature [17].

Table 4. Coating pore resistance, R_c, of the Ag/HAP and Ag/HAP/Gr coatings on titanium surface

Tabela 4. Otpornost u porama prevlake, R_c, za Ag/HAP i Ag/HAP/Gr prevlake na površini titana

Coating	*t*/h	R_c / kΩ cm^2
Ag/HAP/Gr	1	6.12
	8	5.69
	24	3.51
	72	2.48
	168	3.05
	504	73.9
	576	-
Ag/HAP	1	9.50
	8	12.0
	24	90.3
	72	-

For Ag/HAP/Gr coating, during first 3 days, coating pores were filled with SBF, which can be detected by decreasing of R_c value from 6.12 to 2.48 kΩ cm^2 (Table 4). After 7 days, new apatite layer formation begin to occur which was detected by increasing in R_c to the value of 3.05 kΩ cm^2 . Deposition of a newly formed carbonated HAP on the top of Ag/HAP/Gr coating occured after 21 days, when R_c parameter reached the value of 73.9 kΩ cm^2. Based on this experimental results, Ag/HAP/Gr coating surface represents the site of nucleation and growth of new apatite layer – carbonated HAP. After 24 days, Ag/HAP/Gr coating lost its adhesion property.

After initial 8 hours period the new apatite layer formation occured on the top of the Ag/HAP coating, which can be confirmed by increase in R_c value from 9.5 kΩ cm^2 (after 1h immersion) to 12.0 kΩ cm^2 (after 8 h immersion). Contrary to the Ag/HAP/Gr, Ag/HAP coating lost its corrosion stability after 72 hours due to coating adhesion loss.

Based on the EIS data, it could be concluded that Ag/HAP/Gr coating exhibited superior biomimetic mineralization compared to its Ag/HAP counterpart due to graphene incorporation in hydroxyapatite matrix in composite Ag/HAP/Gr coating.

Cytotoxicity of Ag/HAP and Ag/HAP/Gr coatings was determined by MTT test against healthy PBMC. The evaluated Ag/HAP coating had shown almost no cytotoxic effect judging by survival of PBMCs 94.6±4.2 % [51]. For Ag/HAP/Gr sample cell survival of PBMCs, was 79.6±11.2%. In the case of Gr containing sample, examination of cytotoxic effects showed mild decrease in survival of healthy immunocompetent PBMC compared to the control cell sample. However, according to the materials classification [61], Ag/HAP and Ag/HAP/Gr coatings displayed no cytotoxic effects against targeted PBMCs.

The antibacterial activity of Ag/HAP and Ag/HAP/Gr coating was tested against *S. aureus* TL and *E. coli* (ATCC 25922) quantitavely by monitoring changes in the viable number of bacterial cells in suspension [17,51]. Antibacterial activity of the graphene-free Ag/HAP coating against *S. aureus* TL was noticed immediately after inoculation and the same trend was clearly evidenced throughout the 24 h duration of the experiment. Similar antimicrobial activity was noticed for the Ag/HAP/Gr coating. Namely, antimicrobial activity of the Ag/HAP/Gr coating could be noticed immediately after inoculation of the samples and subsequently one logarithmic unit reduction of cell viability is achieved after only 1 hour of incubation. Calculations based on initial number of cells in suspensions and 1h post-incubation revealed that Ag/HAP/Gr coating exhibited reduction of both bacteria, *S. aureus* TL (72.9% percentage of cell reduction) and *E. coli* (68.4% percentage of cell reduction). Graphene-based coating exhibited strong antibacterial activity also after 3 hours of exposure, therefore suppressing harmful biofilm formation. Exactly as in the case of Ag/HAP coating, after 24 hours, analyzed Ag/HAP/Gr samples did not contain any viable cell or visible colony even when samples were taken directly from the suspensions. An immediate silver ion release for both Ag/HAP and Ag/HAP/Gr coatings provided for the imminent drop in CFU numbers, which fits well with bactericidal properties necessary for prevention of biofilm formation.

4. GRAPHENE DOPED HYDROXYAPATITE/CHITOSAN COATINGS

Three different ethanol suspensions were prepared to obtain cataphoretically deposited HAP coating (1 wt.% of HAP), HAP/CS coating (1 wt.% of HAP and 0.05 wt.% of CS) and HAP/CS/Gr coating (1 wt.% of HAP, 0.05 wt.% of CS and 0.01 wt.% of Gr) [13].

Fig. 4 shows FE-SEM micrographs of HAP, HAP/CS and HAP/CS/Gr coatings deposited on titanium. Sphere-like agglomerates of different sizes were noticeable in HAP coating FE-SEM micrograph (Fig. 4a). FE-SEM micrograph of the HAP/CS coating (Fig. 4b) revealed spherically shaped HAP particles embedded in a chitosan polymer matrix. Incorporation of graphene, as nanofiler, caused significant change in the morphology of the HAP/CS/Gr coating (Fig. 4c) with respect to the morphology of HAP and

HAP/CS coatings. Namely, curved graphene sheets are well dispersed in HAP/CS matrix as denoted by white arrows in Fig 4c. Addition of chitosan and graphene to composite coatings HAP/CS (Fig. 4b) and HAP/CS/Gr (Fig. 4c) altered porosity, with respect to the HAP coating (Fig. 4a).

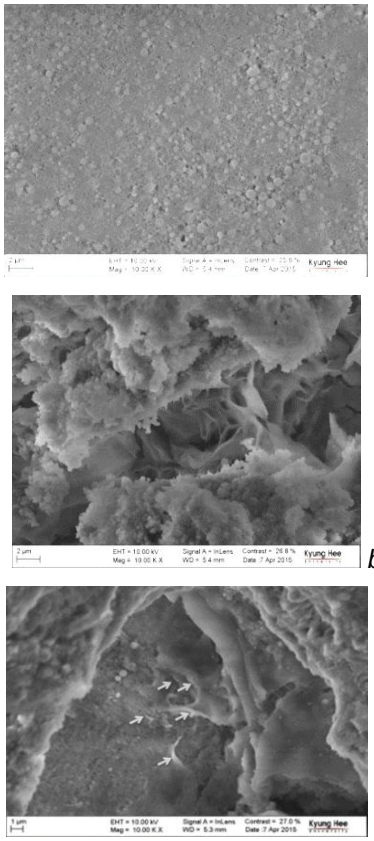

a) b) c)

Figure 4. FE-SEM micrographs of the HAP (a), HAP/CS (b) and HAP/CS/Gr (c) coatings on titanium surface, magnification 10000x.

Slika 4. FE-SEM mikrofotografije HAP (a), HAP/CS (b) i HAP/CS/Gr (c) prevlaka na površini titana, uvećanje 10000x.

Porous structure with micro-cracks is observed in HAP/CS, while addition of graphene contributed to the more compact surface which might be a consequence of the bonding between CS and Gr, or bonding between HAP and Gr. Addition of graphene sheets may have an inhibitory effect on the formation of cracks at the chitosan-graphene interface [44]. Moreover, sphere-like HAP particles were smoothly distributed in the chitosan-graphene matrix of HAP/CS/Gr, due to high specific surface area of graphene nanosheets, and increased contact area.

The FT-IR wavenumbers and corresponding assignments of absorption bands for HAP, HAP/CS and HAP/CS/Gr coatings are represented in Table 5. In FTIR spectra for HAP coating [13] characteristic bands at 562 cm^{-1} and 599 cm^{-1} were attributed to the P-O bond in the phosphate group (ν_4 vibrational mode), while bands at the 960, 1020, and 1086 cm^{-1} could be assigned to bond vibration in PO_4^{3-} ions. The presence of OH^- groups in the HAP structure was evidenced by few characteristic bands, i.e. band at 630 cm^{-1} (assigned to the vibrational mode of the OH^- group in the HAP structure [43,62]), and band at around 3417 cm^{-1} (attributed to the stretching vibration of the free OH^- group [63]). The band at 875 cm^{-1} is assigned to the P-(OH) stretching vibration in the HPO_4^{2-} phosphate group [16,64]. Bands at 1407 and 1462 cm^{-1} correspond to the ν_3 asymmetrical stretching vibration of the CO_3^{2-} group [13,17,43].

FT-IR spectra for HAP/CS and HAP/CS/Gr composite coatings exhibited all the characteristic bands that have been reported for the pure HAP coating [13]. Moreover, bands assigned to stretching vibrations of hydroxyl groups, appeared at around 3380 and 3381 cm^{-1} for HAP/CS and HAP/CS/Gr coatings, respectively, slightly shifted toward lower wavenumbers compared to stretching vibrations of free OH^- group in HAP (around 3417 cm^{-1}). This indicates the formation of hydrogen bonds between HAP and chitosan. Chemical interconnection between HAP and chitosan was also confirmed through the disappearing of characteristic band for chitosan structure [13]. On the other side, HAP/CS FTIR spectrum revealed a new band at 1640 cm^{-1} (amide I band), assigned to the stretching of the C=O group in CS structure). The existence of graphene in HAP/CS/Gr composite was confirmed by new band at 1578 cm^{-1} that can be assigned to the skeletal vibration of graphene nanosheets [13,17,48].

XRD patterns for HAP, HAP/CS and HAP/CS/Gr coatings showed diffraction peaks corresponding to pure HAP, while neither chitosan nor graphene in the HAP/CS/Gr coating were observed, most probably due to low CS and Gr content in the starting suspensions or significant overlapping with HAP characteristic peaks [13]. Interactions of graphene and/or chitosan with HAP were detected through the shifting of HAP characteristic diffraction maximums to higher 2θ, in the case of HAP/CS, or lower 2θ angle in the case of HAP/CS/Gr. Interaction between HAP and CS in HAP/CS coating can be explained through the formation of intermolecular hydrogen bonds and coordination bonds between Ca^{2+} at the surface of HAP crystals and–OH and NH_2 groups from CS [13]. Introduction of CS to HAP coating significantly reduced the crystallite domain size of HAP contrary to HAP/CS/Gr where after the introduction of the graphene crystallite domain size of HAP increased [13]. Additionally, the unit cell parameters *a* and c,

also unit cell volume, both increased. It can be concluded that this was due to the facilitated intercalation of HAP nanoparticles in the polymer network reinforced by graphene [13,17,65]. It has been reported that graphene, due to its large surface area is capable of forming strong bonds with CS [66], acting as a nanofiller throughout the polymer matrix. In addition, graphene connects to HAP by Van der Waals interactions.

Table 5. FT-IR absorption bands of the HAP, HAP/CS and HAP/CS/Gr coatings on titanium surface.

Tabela 5. FT-IR apsorpcione trake za HAP, HAP/CS i HAP/CS/Gr prevlake na površini titana.

Coating	Group	Wavenumber / cm^{-1}	Assignment [13,17,43,48,63,64]
HAP	PO_4^{3-}	562, 599	P-O bond in the phosphate group
		960, 1020, 1086	bond vibration in PO_4^{3-} ions
	HPO_4^{2-}	875	P-(OH) stretching vibration
	CO_3^{2-}	1407, 1462	asymmetrical stretching vibration of the CO_3^{2-} group
	OH^-	630	vibration of the OH^- group in the HAP structure
		3417	stretching vibration of the free OH^- group
HAP/CS	PO_4^{3-}	562, 599	P-O bond in the phosphate group
		960, 1020, 1086	bond vibration in PO_4^{3-} ions
	HPO_4^{2-}	875	P-(OH) stretching vibration
	CO_3^{2-}	1407, 1462	asymmetrical stretching vibration of the CO_3^{2-} group
	OH^-	630	vibration of the OH^- group in the HAP structure
		3380	stretching vibration of the free OH^- group
	C=O	1640 cm^{-1}	stretching of the C=O group in CS structure
HAP/CS/Gr	PO_4^{3-}	562, 599	P-O bond in the phosphate group
		960, 1020, 1086	bond vibration in PO_4^{3-} ions
	HPO_4^{2-}	875	P-(OH) stretching vibration
	CO_3^{2-}	1407, 1462	asymmetrical stretching vibration of the CO_3^{2-} group
	OH^-	630	vibration of the OH^- group in the HAP structure
		3381	stretching vibration of the free OH^- group
	C=C	1578	skeletal vibration of graphene

XPS results, for all three coatings, confirmed the calcium (originated from HAP) and titanium (originated from the substrate) presence [67,68]. The appearance of C1s signal, characteristic for carbon structures, confirmed the presence of both chitosan and graphene in HAP/CS and HAP/CS/Gr coatings. Moreover, the much higher element content of carbon in HAP/CS/Gr coating (32.5 %), compared to HAP/CS (18.7 %) indicated the successful incorporation of graphene sheets in the HAP/CS/Gr coating. Also, the presence of aromatic hydrocarbons was detected [60], which is consistent with the honeycomb structure of graphene. HAP/CS and HAP/CS/Gr composite coatings have Ca/P ratios of 1.64 and 1.74, respectively, which are close to the ratio of the pure HAP coating (1.66).

The thermal decomposition of HAP/CS and HAP/CS/Gr composite coatings, in the temperature range from 30 to 1000 °C, occurred in several stages [13] that could be described as follows: loss of adsorbed water on the coating surface, release of crystalline water, decomposition of chitosan, decomposition of carbonate ions from HAP structure, decomposition of Gr nanosheets (HAP/CS/Gr coating) and finally dehydroxylation and decomposition of HAP. The total weight loss in the temperature range 30 °C – 1000 °C was 21.76 wt.% for HAP/CS and 20.97 wt.% for HAP/CS/Gr coating. The smaller weight loss in the case of HAP/CS/Gr coating indicated slightly increased thermal stability of HAP/CS/Gr coating, compared to HAP/CS. This can be explained by the reinforcement of composite coating through the graphene addition as nanofiller.

Bioactivity was demonstrated by the nucleation and growth of carbonated HAP on the electrophoretically deposited HAP, HAP/CS, and HAP/CS/Gr surfaces, with crystallite domain sizes of 426 Å, 251 Å, and 220 Å, respectively [13]. The smallest HAP crystallites were grown on coatings with incorporated graphene sheets after immersion in SBF, due to the nucleation of HAP crystals on either the graphene walls or the cross-sections of graphene multi-sheets. The small crystallite domain size of newly formed apatite could be attributed to strong electrostatic interactions between functional groups at the coating surface and mineral ions, which promotes the nucleation of carbonated HAP on HAP, HAP/CS and HAP/CS/Gr coatings. The

biomineralization process, i.e. the growth of HAP on the coating surface after immersion in SBF, depends on the availability of functional groups. Hydroxyl and phosphate ions in HAP upon SBF immersion caused HAP surface to become negatively charged and consequently attract Ca^{2+} ions. That high calcium consumption resulted in the precipitation of calcium phosphates. At the same time HAP dissolves, increasing the concentration of calcium and phosphate ions in solution and leading to the precipitation of HAP. The dissolution and precipitation of calcium phosphates in SBF is a reversible reaction. Graphene promoted the deposition of HAP by attracting calcium ions, due to its negative surface charge arising from the large number of *p*-electrons in sp^2 hybrid orbitals. Presence of amino and hydroxyl groups in chitosan influenced HAP nucleation and crystallization through an electrostatic interaction with calcium ions. Based on experimental data, HAP/CS and HAP/CS/Gr composite coatings enable nucleation and growth of HAP, therefore facilitating bonding between the natural bone and the implant.

The corrosion stability of HAP, HAP/CS and HAP/CS/Gr coatings in SBF solution at 37 °C was monitored using EIS measurements. The Nyquist plots of titanium coated with HAP/CS and HAP/CS/Gr for periods up to 20 days of immersion in SBF are discussed in literature in details [13]. The EIS data were fitted using the equivalent electrical circuit (EECs) represented in Fig. 2a for HAP and HAP/CS and in Fig. 5 for HAP/CS/Gr coating.

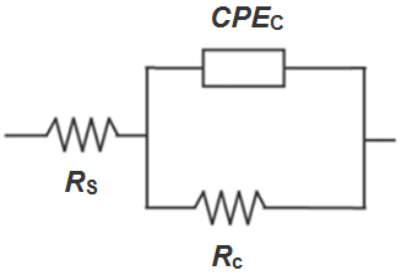

Figure 5. Equivalent electrical circuit used for impedance plots fitting of the HAP/CS/Gr coating on titanium surface during different immersion times in SBF at 37 ºC

Slika 5. Ekvivalentno električno kolo korišćeno za fitovanje impedansnih dijagrama za HAP/CS/Gr prevlaku na površini titana, tokom vremena delovanja SBF na 37 ºC

Obtained results indicated that SBF solution diffused into the coating pores. Thus, the ion exchange of Ca^{2+} and PO_4^{2-} ions with the SBF solution induced the dissolution of hydroxyapatite on the coating surface. Simultaneously, dissolution of HAP caused an increase in the ionic concentration of the electrolyte, prompting the formation of a new apatite phase on the coating surface. Generally, the calcium phosphate dissolution in SBF is a reversible reaction, occurring simultaneously with spontaneous precipitation [14,69]. It was shown that, after 28 days, improved bioactivity was observed due to the growth of a carbonated apatite layer, which can be confirmed by increase in R_c values from 105 to 637 Ωcm^2 for HAP, from 105 to 205 Ωcm^2 for HAP/CS, and from 192 to 484 Ωcm^2 for HAP/CS/Gr. This was also confirmed by FE-SEM and XRD [13]. This growth of a new apatite phase in physiological media is desirable, as it indicates that HAP from the coating is transformed to bone-like apatite, which enables formation of stable bonds to natural bone in the human body [70].

Table 6. Coating pore resistance, R_c, of the HAP, HAP/CS and HAP/CS/Gr coatings on titanium surface.

Tabela 6. Otpornost u porama prevlake, R_c, za HAP, HAP/CS i HAP/CS/Gr prevlake na površini titana.

Coating	*t*/h	R_c / Ω cm^2
HAP	96	105
	672	637
HAP/CS	168	105
	672	205
HAP/CS/Gr	165	192
	672	484

The cytotoxic effect of HAP, HAP/CS, and HAP/CS/Gr coatings was determined by MTT testing against PBMC. Spectrophotometric determination of optical density (OD) value for formazan–DMSO solution is considered to be proportional to the number of living cells. Investigations showed a mild decrease in the survival of healthy immunocompetent PBMC compared to the control sample, i.e. 84 % for HAP, 69 % for HAP/CS and 67 % for HAP/CS/Gr [13]. According to the literature classification [61], HAP, HAP/CS, and HAP/CS/Gr coatings could be listed as non-cytotoxic against targeted PBMCs within the margin of error. However, when cells were stimulated for proliferation, intensified drop in cell viability was observed for all investigated coatings.

Antibacterial activity of HAP, HAP/CS, and HAP/CS/Gr coatings on Ti substrate was tested against microorganisms that are responsible for the most of inter-hospital infections. Taking into consideration structural differences of the bacterial cell wall, *S.aureus* (Gram-positive bacterium) and *E.coli* (Gram-negative bacterium) were investigated

by monitoring changes in the viable number of bacterial cells in suspension during 24 h period. Antibacterial activity of HAP, HAP/CS, and HAP/CS/Gr coatings was tested against *S.aureus* TL and *E.coli* strains in sterile phosphate buffer, respectively [13].

Antibacterial effects were evaluated immediately after inoculation, followed by aliquoting after 1 h, 3 h and 24 h of incubation. Cell counts were slightly retained even up to 3 h post incubation for all samples when compared to the initial number of cells in the suspension. This effect was slightly more pronounced for the samples tested against *S.aureus*. Viability of *E.coli*, however, was less perturbed by the presence of HAP, HAP/CS, and HAP/CS/Gr coated Ti foils [13]. Unfortunately, after 24 h, all coatings exhibited no reduction of *S.aureus* TL or *E .coli* cell counts, clearly demonstrating that at such low concentrations of CS, its antibacterial potential could not be expressed.

5. CONCLUSIONS

Bioactive pure HAP and composite Ag/HAP, HAP/Gr, Ag/HAP/Gr, HAP/CS and HAP/CS/Gr coatings were produced by electrophoretic deposition on titanium substrate using constant voltage method.

Graphene incorporation in HAP/Gr, Ag/HAP/Gr and HAP/CS/Gr coatings was evidenced by FT-IR and XPS spectra, and facilitated more uniform coating surface with less microcracks, proved by FE-SEM. The Ca/P ratio, calculated from XPS analysis) for all coatings is similar to the stoichiometric Ca/P ratio. The greater thermal stability of graphene-based coatings compared to the graphene-free coatings was confirmed by TGA, emphasizing improvements brought in by graphene addition. EIS analysis clearly confirmed the bioactivity of all coatings, i.e. the formation of an apatite layer after soaking in SBF. Based on the EIS data, the graphene-based coatings exhibited superior biomimetic mineralization compared to the graphene-free coatings as well as greater corrosion stability in SBF solution.

In vitro cytotoxicity evaluation indicated all deposited coatings as non-cytotoxic against PBMC. No antibacterial effect of HAP and HAP/Gr coatings could be observed against two common types of bacteria, *S.aureus* TL and *E.coli*, while Ag/HAP and Ag/HAP/Gr coatings exhibited strong antibacterial activity against *S.aureus* and *E.coli* after only 3 hours of exposure, therefore suppressing harmful biofilm formation. Unfortunately, the amount of transferred CS in HAP/CS and HAP/CS/Gr was not sufficient for pronounced antibacterial effect and even after 24 h, all coatings exhibited no reduction of *S.aureus* TL or *E.coli* cell counts.

Acknowledgments

The authors are grateful to the Ministry of Education, Science and Technological Development of Serbia for financial support, Grant No. III45019. This work was also supported by the Basic Science Research Program through the National Research Foundation of Korea (NRF) funded by the Ministry of Education, Science and Technology (project No: 2016R1A2B4016034).

Author disclosure statement

The authors confirm that this article content has no conflict of interest.

6. REFERENCES

[1] M.S.Djošić, V.B.Mišković-Stanković, S.Milonjić, Z.M. Kačarević-Popović, N.Bibić, J.Stojanović (2008) Electrochemical synthesis and characterization of hydroxyapatite powders, Mater. Chem. Phys., 111, 137–142.

[2] N.Y.Mostafa (2005) Characterization, thermal stability and sintering of hydroxyapatite powders prepared by different routes, Mater. Chem. Phys., 94, 333–341.

[3] M.S. Djošić, V.Panić, J.Stojanović, M.Mitrić, V.B. Miskovic-Stankovic (2012) The effect of applied current density on the surface morphology of deposited calcium phosphate coatings on titanium, Colloids Surf. A, 400, 36–43.

[4] V.B.Mišković-Stanković (2014) Electrodeposition and Surface Finishing: Fundamentals and Applications, Modern Aspects of Electrochemistry 57, Springer Science+Business Media, New York, USA, Chapter 3, p. 133-216.

[5] K.Singh, P.Prasher, K.Kaur (2017) Surface modification of dental implants, Indian J. Compr. Dent. Care., 7, 10–14.

[6] K. Shemtov-Yona, D.Rittel (2015) An Overview of the Mechanical Integrity of Dental Implants, Biomed. Res. Int. 2015, 11 pages.

[7] A.Stoch, A.Brozek, G.Kmita, J.Stoch, W. Jastrzebski, A.Rakowska (2001) Electrophoretic coating of hydroxyapatite-boron nitride nanocomposites on titanium implants, J. Mol. Struct., 596, 191–200.

[8] S. Eftekhari, I. El Sawi, Z.S. Bagheri, G. Turcotte, H. Bougherara (2014) Fabrication and characterization of novel biomimetic PLLA/cellulose/ hydroxyapatite nanocomposite for bone repair applications, Mater. Sci. Eng. C., 39, 120–125.

[9] R.S.Pillai, M.Frasnelli, V.M.Sglavo (2018) HA/β-TCP plasma sprayed coatings on Ti substrate for biomedical applications, Ceram. Int., 44, 1328–1333.

[10] C.Domínguez-Trujillo, E.Peón, E.Chicardi, H. Pérez, J.A.Rodríguez-Ortiz, J.J.Pavón, J.García-Couce,

J.C.Galván, F.García-Moreno, Y.Torres (2018) Sol-gel deposition of hydroxyapatite coatings on porous titanium for biomedical applications, Surf. Coat. Tech., 333, 158–162.

[11] A. Zaharia, V. Muşat, E.M. Anghel, I. Atkinson, O.C. Mocioiu, M. Buşilă, V.G. Pleşcan (2017) Biomimetic chitosan-hydroxyapatite hybrid biocoatings for enamel remineralization, Ceram. Int., 43, 11390–11402.

[12] G.Popescu-Pelin, F.Sima, L.E.Sima, C.N. Mihailescu, C.Luculescu, I.Iordache, M.Socol, G. Socol, I.N. Mihailescu (2017) Hydroxyapatite thin films grown by pulsed laser deposition and matrix assisted pulsed laser evaporation: Comparative study, Appl. Surf. Sci., 418, 580–588.

[13] M. Đošić, S. Eraković, A. Janković, M. Vukašinović-Sekulić, I.Z.Matić, J.Stojanović, K.Y.Rhee, V. Mišković-Stanković, S.-J.Park (2017) In vitro investigation of electrophoretically deposited bioactive hydroxyapatite/chitosan coatings reinforced by graphene, J. Ind. Eng. Chem., 47, 336–347.

[14] M.S.Djošić, M.Mitrić, V.B.Mišković-Stankovic (2015) The porosity and roughness of electrodeposited calcium phosphate coatings in simulated body fluid, J. Serb. Chem. Soc., 80, 237–251.

[15] A.Janković, S. Eraković, A. Dindune, D. Veljović, T. Stevanović, D. Janaćković, V. Miskovic-Stankovic (2012) Electrochemical impedance spectroscopy of a silver-doped hydroxyapatite coating in simulated body fluid used as a corrosive agent, J. Serb. Chem. Soc., 77, 1609–1623.

[16] A.Janković, S.Eraković, M.Mitrić, I.Z.Matić, Z.D. Juranić, G.C.P. Tsui, C. Tang, V. Mišković-Stanković, K.Y. Rhee, S.J. Park (2015) Bioactive hydroxyapatite/graphene composite coating and its corrosion stability in simulated body fluid, J. Alloys Compd., 624, 148–157.

[17] A. Janković, S. Eraković, M. Vukašinović-Sekulić, V. Mišković-Stanković, S.J. Park, K.Y. Rhee (2015) Graphene-based antibacterial composite coatings electrodeposited on titanium for biomedical applications, Prog. Org. Coat., 83, 1–10.

[18] D.Alves Cardoso, J.A.Jansen, S.C.G. Leeuwenburgh (2012) Synthesis and application of nanostructured calcium phosphate ceramics for bone regeneration, J. Biomed. Mater. Res. B, 100B, 2316–2326.

[19] N. Pramanik, D. Mishra, I. Banerjee, T.K. Maiti, P. Bhargava, P. Pramanik (2009) Chemical synthesis, characterization, and biocompatibility study of hydroxyapatite/chitosan phosphate nanocomposite for bone tissue engineering applications, Int. J. Biomater., ID 512417.

[20] R.E. McMahon, L. Wang, R. Skoracki, A.B. Mathur (2013) Development of nanomaterials for bone repair and regeneration, J. Biomed. Mater. Res. B, 101 B, 387–397.

[21] A.Simchi, E.Tamjid, F.Pishbin, A.R. Boccaccini (2011) Recent progress in inorganic and composite coatings with bactericidal capability for orthopaedic applications, Nanomed. Nanotechnol., 7, 22–39.

[22] F.Gebhardt, S.Seuss, M.C.Turhan, H.Hornberger, S.Virtanen, A.R. Boccaccini (2012) Characterization of electrophoretic chitosan coatings on stainless steel, Mater. Lett., 66, 302–304.

[23] S.Mahmoodi, L.Sorkhi, M.Farrokhi-Rad, T.Shahrabi (2013) Electrophoretic deposition of hydroxyapatite-chitosan nanocomposite coatings in different alcohols, Surf. Coat. Tech., 216, 106–114.

[24] F.Batmanghelich, M.Ghorbani (2013) Effect of pH and carbon nanotube content on the corrosion behavior of electrophoretically deposited chitosan-hydroxyapatite-carbon nanotube composite coatings, Ceram. Int., 39, 5393–5402.

[25] D.Zhitomirsky, J.A.Roether, A.R.Boccaccini, I. Zhitomirsky (2009) Electrophoretic deposition of bioactive glass/polymer composite coatings with and without HA nanoparticle inclusions for biomedical applications, J. Mater. Process. Tech., 209, 1853–1860.

[26] M.Cheong, I.Zhitomirsky (2008) Electrodeposition of alginic acid and composite films, Colloids Surf. A, 328, 73–78.

[27] C.E.Tanase, M.I.Popa, L.Verestiuc (2009) Chitosan-hydroxyapatite composite obtained by biomimetic method as new bone substitute, Proc. - 2009 Adv. Technol. Enhanc. Qual. Life, AT-EQUAL 2009., 19, 42–46.

[28] A.Lahiji, A.Sohrabi, D.S.Hungerford, C.G.Frondoza (2000) Chitosan supports the expression of extracellular matrix proteins in human osteoblasts and chondrocytes, J. Biomed. Mater. Res., 51, 586–595.

[29] V. Mišković-Stanković, A. Janković, S. Eraković, K. Yop Rhee (2014) Graphene Based Biomedical Composite Coatings Produced by Electrophoretic Deposition on Titanium, ECTJ, 17, 3-15.

[30] Y. Liu, Z.Dang, Y.Wang, J.Huang, H.Li (2014) Hydroxyapatite/graphene-nanosheet composite coatings deposited by vacuum cold spraying for biomedical applications: Inherited nanostructures and enhanced properties, Carbon, 67, 250–259.

[31] L.Zhang, W.Liu, C. Yue, T Zhang, P. Li, Z.Xing, Y. Chen (2013) A tough graphene nanosheet/hydroxyapatite composite with improved in vitro biocompatibility, Carbon, 61, 105–115.

[32] A. Chavez-Valdez, M.S.P. Shaffer, A.R. Boccaccini (2013) Applications of graphene electrophoretic deposition. A review, J. Phys. Chem. B., 117, 1502–1515.

[33] G.M.Neelgund, A.Oki, Z.Luo (2013) In situ deposition of hydroxyapatite on graphene nanosheets, Mater. Res. Bull., 48, 175–179.

[34] M.Belmonte, C.Ramírez, J.González-Julián, J. Schneider, P. Miranzo, M.I. Osendi (2013) The beneficial effect of graphene nanofillers on the tribological performance of ceramics, Carbon, 61, 431–435.

[35] M.Kalbacova, A.Broz, J.Kong, M.Kalbac (2010) Graphene substrates promote adherence of human osteoblasts and mesenchymal stromal cells, Carbon, 48, 4323–4329.

[36] W. Hu, C. Peng, W. Luo, M. Lv, X. Li, D. Li, Q. Huang, C. Fan (2010) Graphene-Based Antibacterial Paper, ASC Nano, 4, 4317–4323.

[37] H. Liu, P. Xi, G. Xie, Y. Shi, F. Hou, L. Huang, F. Chen, Z. Zeng, C. Shao, J. Wang (2012) Simultaneous reduction and surface functionalization of graphene oxide for hydroxyapatite mineralization, J. Phys. Chem. C., 116, 3334–3341.

[38] V. Mourino, J.P. Cattalini, A.R. Boccaccini (2012) Metallic ions as therapeutic agents in tissue engineering scaffolds: an overview of their biological applications and strategies for new developments, J. R. Soc. Interface, 9, 401–419.

[39] P.N. Lim, L. Chang, E.S. Thian (2015) Development of nanosized silver-substituted apatite for biomedical applications: A review, Nanomed. Nanotechnol., 11, 1331–1344.

[40] I.S. Lee, C.N. Whang, K.S. Oh, J.C. Park, K.Y. Lee, G.H. Lee, S.M. Chung, X.D. Sun (2006) Formation of silver incorporated calcium phosphate film for medical applications, Nucl. Instrum. Meth. B, 242, 45–47.

[41] X. Pang, I. Zhitomirsky (2008) Electrodeposition of hydroxyapatite-silver-chitosan nanocomposite coatings, Surf. Coat. Tech., 202, 3815–3821.

[42] S. Erakovic, D. Veljovic, P.N. Diouf, T.Stevanovic, M. Mitric, S.Milonjic, V.B.Miskovic-Stankovic (2009) Electrophoretic Deposition of Biocomposite Lignin/Hydroxyapatite Coatings on Titanium, Int. J. Chem. React. Eng., 7, 1-14.

[43] V. Mišković-Stanković, S. Eraković, A. Janković, M. Vukašinović-Sekulić, M. Mitrić, Y.C. Jung, S.J. Park, K.Y. Rhee (2015) Electrochemical synthesis of nanosized hydroxyapatite/graphene composite powder, Carbon Lett., 16, 233–240.

[44] M. Li, Q. Liu, Z. Jia, X. Xu, Y. Shi, Y. Cheng, Y. Zheng, T. Xi, S. Wei (2013) Electrophoretic deposition and electrochemical behavior of novel graphene oxide-hyaluronic acid-hydroxyapatite nanocomposite coatings, Appl. Surf. Sci., 284, 804–810.

[45] S.Baradaran, E.Moghaddam, W.J.Basirun, M. Mehrali, M.Sookhakian, M.Hamdi, M.R.N. Moghaddam, Y.Alias (2014) Mechanical properties and biomedical applications of a nanotube hydroxyapatite-reduced graphene oxide composite, Carbon, 69, 32–45.

[46] S.Eraković, A.Janković, C.Ristoscu, L.Duta, N. Serban, A.Visan, I.N.Mihailescu, G.E.Stan, M. Socol, O. Iordache, I.Dumitrescu, C.R. Luculescu, D.Janaćković, V.Miškovic-Stanković (2014) Antifungal activity of Ag:hydroxyapatite thin films synthesized by pulsed laser deposition on Ti and Ti modified by TiO_2 nanotubes substrates, Appl. Surf. Sci., 293, 37–45.

[47] C.C.Wu, S. Te Huang, T.W.Tseng, Q.L.Rao, H.C. Lin (2010) FT-IR and XRD investigations on sintered fluoridated hydroxyapatite composites, J. Mol. Struct., 979, 72–76.

[48] P. Lian, X. Zhu, S.Liang, Z.Li, W.Yang, H.Wang (2010) Large reversible capacity of high quality graphene sheets as an anode material for lithium-ion batteries, Electrochim. Acta., 55, 3909–3914.

[49] Y.Liu, J.Huang, H.Li (2013) Synthesis of hydroxyapatite–reduced graphite oxide nanocomposites for biomedical applications: oriented nucleation and epitaxial growth of hydroxyapatite, J. Mater. Chem. B., 1, 1826-1834.

[50] Y.W. Gu, K.A. Khor, P. Cheang (2004) Bone-like apatite layer formation on hydroxyapatite prepared by spark plasma sintering (SPS), Biomaterials., 25, 4127–4134.

[51] S. Eraković, A. Janković, I.Z. Matić, Z.D. Juranić, M. Vukašinović-Sekulić, T. Stevanović, V. Miskovic-Stankovic (2013) Investigation of silver impact on hydroxyapatite/lignin coatings electrodeposited on titanium, Mater. Chem. Phys., 142, 521–530.

[52] P.N.Chavan, M.M.Bahir, R.U.Mene, M.P. Mahabole, R.S.Khairnar (2010) Study of nanobiomaterial hydroxyapatite in simulated body fluid: Formation and growth of apatite, Mater. Sci. Eng. B Solid-State Mater. Adv. Technol., 168, 224–230.

[53] M.Javidi, S.Javadpour, M.E.Bahrololoom, J.Ma (2008) Electrophoretic deposition of natural hydroxyapatite on medical grade 316L stainless steel, Mater. Sci. Eng. C., 28, 1509–1515.

[54] E.Mavropoulos, A.M.Costa, L.T.Costa, C.A. Achete, A.Mello, J.M.Granjeiro, A.M.Rossi (2011) Adsorption and bioactivity studies of albumin onto hydroxyapatite surface, Composites Part B, 83, 1–9.

[55] K.P.Sanosh, M.C.Chu, A.Balakrishnan, Y.J.Lee, T.N.Kim, S.J.Cho (2009) Synthesis of nano hydroxyapatite powder that simulate teeth particle morphology and composition, Curr. Appl. Phys., 9, 1459–1462.

[56] L.N.Wang, J.L.Luo (2011) Fabrication and formation of bioactive anodic zirconium oxide nanotubes containing presynthesized hydroxyapatite via alternative immersion method, Mater. Sci. Eng. C., 31, 748–754.

[57] H.Ye, X.Y.Liu, H.Hong (2009) Cladding of titanium/hydroxyapatite composites onto Ti6Al4V for load-bearing implant applications, Mater. Sci. Eng. C., 29, 2036–2044.

[58] Z. Fan, J. Wang, Z. Wang, H. Ran, Y. Li, L. Niu, P. Gong, B. Liu, S. Yang (2014) One-pot synthesis of graphene/hydroxyapatite nanorod composite for tissue engineering, Carbon, 66, 407–416.

[59] S. Erakovic, A. Jankovic, D. Veljovic, E. Palcevskis, M. Mitric, T. Stevanovic, V. Miskovic-Stankovic (2013) Corrosion Stability and Bioactivity in Simulated Body Fluid of Silver/Hydroxyapatite and Silver/Hydroxyapatite/Lignin Coatings on Titanium Obtained by Electrophoretic Deposition, J. Phys. Chem. B. 117, 1633–1643.

[60] K.M. Watling, J.F. Parr, L. Rintoul, C.L. Brown, L.A. Sullivan (2011) Raman, infrared and XPS study of bamboo phytoliths after chemical digestion, Spectrochim. Acta - Part A Mol. Biomol. Spectrosc., 80, 106–111.

[61] G. Sjögren, G. Sletten, J.E.E. Dahl (2000) Cytotoxicity of dental alloys, metals, and ceramics

assessed by Millipore filter, agar overlay, and MTT tests, J. Prosthet. Dent., 84, 229–236.
[62] J. Reyes-Gasga, E.L. Martínez-Piñeiro, G. Rodríguez-Álvarez, G.E. Tiznado-Orozco, R. García-García, E.F. Brès (2013) XRD and FTIR crystallinity indices in sound human tooth enamel and synthetic hydroxyapatite, Mater. Sci. Eng. C. 33, 4568–4574.
[63] N. Angelescu, D.N. Ungureanu, F. V Anghelina (2011) Synthesis and characterization of hydroxyapatite obtained in different experimental conditions, Sci. Bull. Valahia Univ. Mater. Mech., 6 (9), 15-18.
[64] M.R. Nikpour, S.M. Rabiee, M. Jahanshahi (2012) Synthesis and characterization of hydroxyapatite/ chitosan nanocomposite materials for medical engineering applications, Compos. Part B Eng., 43, 1881–1886.
[65] M. Li, Y. Wang, Q. Liu, Q. Li, Y. Cheng, Y. Zheng, T. Xi, S. Wei (2013) In situ synthesis and biocompatibility of nano hydroxyapatite on pristine and chitosan functionalized graphene oxide, J. Mater. Chem. B., 1, 475–484.
[66] K. Bustos-Ramírez, A.L. Martínez-Hernández, G. Martínez-Barrera, M. de Icaza, V.M. Castaño, C. Velasco-Santos (2013) Covalently bonded chitosan on graphene oxide via redox reaction, Materials (Basel)., 6, 911–926.
[67] A. Roguska, M. Pisarek, M. Andrzejczuk, M. Dolata, M. Lewandowska, M. Janik-Czachor,(2011) Characterization of a calcium phosphate-TiO2 nanotube composite layer for biomedical applications, Mater. Sci. Eng. C., 31, 906–914.
[68] E.C. Victoria, F.D. Gnanam (2002) Synthesis and Characterisation of Biphasic Calcium Phosphate, Trends Biomater. Artif. Organs., 16, 12–14.
[69] Q. Zhang, J. Chen, J. Feng, Y. Cao, C. Deng, X. Zhang (2003) Dissolution and mineralization behaviors of HA coatings, Biomaterials., 24, 4741–4748.
[70] F. Barrère, C.M. van der Valk, R. a J. Dalmeijer, C. a van Blitterswijk, K. de Groot, P. Layrolle (2003) In vitro and in vivo degradation of biomimetic octacalcium phosphate and carbonate apatite coatings on titanium implants., J. Biomed. Mater. Res. A., 64, 378–387.

IZVOD

BIOKOMPOZITNE PREVLAKE HIDROKSIAPATITA OJAČANE GRAFENOM, DOBIJENE ELEKTROFORETSKIM TALOŽENJEM NA TITANU

Brzi razvoj istraživanja nanomaterijala koji sadrže grafen otkrio je da se njihova izuzetna svojstva mogu koristiti za biomedicinske primene, posebno u inženjerstvu tkiva i kao nosači lekova. U ovom radu su prikazani rezultati istraživanja biokompozitnih prevlaka na bazi hidroksiapatita koje su dobijene elektroforetskim taloženjem na titanskom supstratu i ojačane nanočestičnim grafenom, kao potencijalnih kandidata za implante koštanog tkiva.
Ključne reči: *elektroforetsko taloženje, prevlake, biokompoziti, hidroksiapatit, grafen.*

Pregledni rad
Rad primljen: 26. 04. 2018.
Rad prihvaćen: 19. 05. 2018.
Rad je dostupan na sajtu: www.idk.org.rs/casopis